Time-resolved metabolic footprinting for non-linear modelling of bacterial substrate utilization

Volker Behrends[1,2], Tim MD Ebbels[1], Huw D Williams[2], Jacob G Bundy[1]*

1: Imperial College London, Department of Biomolecular Medicine, Division of Surgery, Oncology, Reproductive Biology, and Anaesthetics, Faculty of Medicine, Sir Alexander Fleming Building, London SW7 2AZ, UK

2: Imperial College London, Department of Life Sciences, Division of Biology, Faculty of Natural Sciences, Sir Alexander Fleming Building, London SW7 2AZ, UK

*Corresponding author.
Email: j.bundy@imperial.ac.uk
Telephone: +44 20 75943039
Fax: +44 20 75943226

Running title: Time-resolved metabolic footprinting

Keywords: metabolomics, *Pseudomonas aeruginosa*, *Burkholderia cepacia* complex, *Escherichia coli*, metabolic footprinting, exometabolome, cystic fibrosis

ABSTRACT

Untargeted profiling of small molecule metabolites from microbial culture supernatants (metabolic footprinting) has great potential as a phenotyping tool. We employed time-resolved metabolic footprinting to compare one *Escherichia coli* and three *Pseudomonas aeruginosa* strains growing on complex media and showed that considering metabolite changes over the whole course of growth provides much more information than taking a single time-point. Most strikingly, there was pronounced selectivity in metabolite uptake, even when the bacteria were growing apparently exponentially, with certain groups of metabolites not taken up until others had been entirely depleted from the medium. Additionally, metabolite excretion showed some complex patterns. Fitting non-linear equations (four-parameter sigmoids) to individual metabolite data allowed us to model these changes for metabolite uptake, and visualize them by back-projecting the curve-fit parameters onto the original growth curves. These 'uptake window' plots clearly demonstrated strain differences, with the uptake of some compounds being reversed in order between different strains. Comparison of an undefined rich medium (LB) with a defined complex medium designed to mimic cystic fibrosis sputum showed many differences, both qualitative and quantitative, with a greater proportion of excreted to utilized metabolites in the defined medium. Extending the strain comparison to a more closely related set of isolates showed it was possible to discriminate two species of the *Burkholderia cepacia* complex based on uptake dynamics alone. We believe time-resolved metabolic footprinting could be a valuable tool for many questions in bacteriology, including isolate comparisons, phenotyping deletion mutants, and as a functional complement to taxonomic classifications.

INTRODUCTION

The increasing speed of gene discovery has exceeded our ability to understand gene function, and one of the bottlenecks is the need for new, high throughput tools to evaluate cellular phenotypes (22). Even in bacterial genomes less than 70% of genes have an assigned putative function and fewer still are characterized biochemically. Metabolic profiling approaches have shown great promise for providing these tools for functional genomics and hypothesis generation (1, 6, 10, 18, 28, 43, 49), because they offer complementary information to transcriptomics and proteomics, in particular giving an integrated picture of information downstream of the genome (51). Various aspects of cellular physiology like the levels of transcripts, proteins or protein activity are altered in response to environmental cues or metabolite concentrations themselves. In return, these changes are amplified in the metabolome to give an accumulated – and highly sensitive – description of the physiological state of the organism or cellular compartment (26, 45, 49). This extends to natural populations that have multiple uncharacterized genetic changes such as an accumulation of mutations, as well as sometimes-extensive genetic differences like pathogenicity islands (21), which may interact to give complex phenotypes. Molecular phylogenetic methods based on gene sequences have proved successful in classifying bacteria into taxonomic groupings, but these may not always correspond to easily identifiable pheno- or ecotypes (29, 33, 48). Hence additional methods for strain assessment that could be related to function would still be valuable.

Metabolomics gives an integrated measurement of cellular phenotype, and is highly suited to quantitative analysis and description. In a microbial context, metabolomics

offers the additional advantage that there is only a single cell type, and little compartmentation (at least in comparison to the equivalent problem in a multicellular organism). However, sampling intracellular metabolites without either changing their relative concentrations or introducing contamination from supernatant metabolites is not straightforward, and research methods are still under active development by different groups (7, 12, 15, 59, 62). In contrast, exometabolome or supernatant profiling ('metabolic footprinting') is simple, and extracellular metabolites can exhibit very large changes in pool size (1, 27, 40, 45). These multiple advantages mean that exometabolome analysis has already been employed for a number of diverse applications, such as phenotyping of both single-gene deletion mutants as well as isolates from natural populations, although so far mostly for fungi rather than bacteria (1, 2, 9, 25, 40, 48).

Because metabolism integrates information from gene expression and a wealth of environmental cues, each organism will exhibit a distinct response, i.e. metabolic pattern that takes into account all these factors. It is therefore unsurprising that these patterns change with growth phase (1, 30). Despite this fact, it is currently common practice to sample only at one or two time-points, mostly the end of growth, in stationary phase (e.g. 48) and/or in mid-exponential phase (41, 52). In contrast, there is ample evidence that cellular biochemistry changes during growth (1, 3, 8, 39). Vertebrate studies have shown that explicitly considering 'through time' responses (metabolic trajectories) adds considerably to the description and understanding of biological events (16, 23, 58). We therefore argue that new approaches that are capable of integrating metabolic phenotypes over a range of conditions could be extremely beneficial for microbiology.

In this study we have developed such an approach and evaluated it by monitoring metabolic changes over the course of time in growing batch cultures. Time Resolved Metabolic Footprinting (TReF) was used to compare the well-studied organisms *Escherichia coli* and *Pseudomonas aeruginosa.* We demonstrate that TReF is considerably more data-rich and informative than sampling at single time points and show the usefulness of the approach in hypothesis generation and as a phenotyping tool. We also show that TReF distinguishes isolates from the closely related *Burkholderia cepacia* complex (Bcc) at the species level for *B. cepacia* and *B. cenocepacia*, which is not the case for single timepoint analysis. The approach is very general and would therefore benefit the broader application of metabolomics to bacterial systems.

MATERIALS AND METHODS

Bacterial strains. We used the following strains in this study: *Escherichia coli* MG1655; the *Pseudomonas aeruginosa* wild type strains PA01 and PA14 (50), *P. aeruginosa* PA0381 *leu*-38 *str*-2, a leucine auxotroph derived from PA01 (17); *B. cenocepacia* LMG 16654, *B. cenocepacia* LMG 16659, *B. cenocepacia* LMG 18830, *B. cenocepacia* LMG 16656 (J2315), *B. cenocepacia* LMG 18863, *B. cepacia* LMG, *B. cepacia* LMG 6963, *B. cepacia* LMG 6988, and *B. cepacia* LMG 18821. Starter cultures for four biological replicates were set up by inoculating single colonies into 5 ml of LB medium (10 g/L tryptone, 5 g yeast extract, 5 g NaCl) and growing overnight at 37°C, shaking at 150 rpm. The growth of PA01 was compared under the same conditions in synthetic cystic fibrosis medium (SCFM), a complex defined medium designed to model nutrient status in sputum (46). These cultures were used to inoculate 20 ml of LB or SCFM in 250 ml conical flasks and then grown for 24 h at 37°C shaking at 150 rpm.

Sampling: 1 ml was taken from the culture at 0, 2, 4, 5, 6, 7, 8, 9, 10, 11, 12, and 24 hours for *E. coli*, *P. aeruginosa* PA01 and all *Burkholderia* strains. The *P. aeruginosa* PA14 and *P. aeruginosa* PA0381 cultures were sampled at 0, 2, 3, 4, 5, 6, 8, 10, 12, 14, 16, and 24 hours. (It should be noted that the total volumes sampled from each culture would potentially change the cell physiology in comparison to an unsampled flask; however, we were not aiming to model an unsampled culture.) For each sample, 0.1 ml was mixed with 0.9 ml culture medium for determination of cell density (OD_{600}). The remainder of the sample was centrifuged (16000 x *g*, RT) and 0.75 ml of the supernatant mixed with 0.2 ml NMR buffer (25 mM sodium azide, 0.25 M phosphate buffer pH 7, and 5 mM sodium 3-trimethylsilyl-2,2,3,3-$^{2}H_4$-propionate

(TSP), in ^2H_2O). The ^2H_2O provided a field frequency lock for the spectrometer and the TSP served as an internal chemical shift reference.

^{1}H NMR measurement: spectra were acquired on a Bruker Avance DRX600 NMR spectrometer (Bruker BioSpin, Rheinstetten, Germany), with a magnetic field strength of 14.1 T and resulting ^{1}H resonance frequency of 600 MHz, equipped with a 5 mm inverse flow probe. Samples were introduced using a Gilson flow-injection autosampler. Spectra were acquired following the approach given in (4). Briefly, a one-dimensional NOESY pulse sequence was used for water suppression; data were acquired into 32 K data points over a spectral width of 12 kHz, with 8 dummy scans and 64 scans per sample, and an additional longitudinal relaxation recovery delay of 3.5 s per scan, giving a total recycle time of 5 s.

Spectral processing and data analysis: Spectra were processed in iNMR 2.5 (Nucleomatica, Molfetta, Italy). Free induction decays were multiplied by an exponential apodization function equivalent to 0.5 Hz line broadening, followed by Fourier transformation. Spectra were manually phased and automated first order baseline correction was applied. Spectral data between –0.5 and 10 ppm were then imported into Matlab 2007b (MathWorks, Cambridge, UK) and normalized to the integral of the TSP signal. Metabolites were assigned using in-house data, the Chenomx NMR Suite 3.1 (Chenomx Inc., Edmonton, Canada) and the Biological Magnetic Resonance Databank metabolomics database (14). Signature peaks, i.e. well-resolved resonances that could be easily assigned to one compound, were identified from the spectra. Difference spectra were calculated in order to eliminate the influence of (non-biological) variation in media composition. For this, the

spectrum at time-point 0 h was subtracted from the spectra of other time-points of the same strain-replicate pair (i.e. all spectra sampled from the same flask). In addition to full resolution spectra, all analyses were carried out on spectra binned integrals representing the dominant resonances detected in fresh, non-inoculated medium. 153 integrals were fitted for LB, and 130 for SCFM. For the heatmap plots, the overall range of the resonance intensity changes was set to one and the changes were expressed relative to the starting values.

Modeling and pattern recognition analysis

We tested two different approaches to monitor the time-dependent changes in metabolite concentration: (a) Linear regression analysis was carried out with both optical density at 600 nm (OD) and time as X variable. A cut-off value for goodness of fit (R^2=0.6) was determined by visual inspection of the fits. (b) Non-linear regression of the data against time using a sigmoid curve model (Eq. 1) was carried out using 'nlinfit' (Matlab statistics toolbox, Matlab). This resulted in fitting each variable with four parameters, the amplitude of the curve, the 'half-life' (t_{50}) and the width of the decrease. Cut-offs for t_{50} (1-24 h), width (0-12 h) and relative error (< 0.6) were imposed.

$$y = \frac{amplitude}{1 + e^{-\frac{x-(t_{50})}{width}}} + offset \qquad [1]$$

The width is defined as the time that elapses for the exponent of e to go from 1 to -1. Growth rate differences (*E. coli* grows faster than the *Pseudomonas* strains) manifest themselves in higher t_{50} values for slower growing than faster growing strains, and these quantitative growth rate effects complicate the elucidation of qualitative

differences that are particularly interesting for strain comparison purposes. Therefore, the sigmoid parameters were corrected for growth-curve bias before pattern recognition: the OD values were also fitted to the same non-linear model (Eq. 1). The amplitude was divided by the amplitude of the OD, and the t_{50} was expressed relative to the t_{50} of the growth curve by subtracting the t_{50} of each individual growth curve and dividing the resulting values by the width of the growth curve (Eq. 2).

$$\Delta t_{50_i} = \frac{t_{50_i} - t_{50_{OD}}}{width_{OD}} \qquad [2]$$

The fitting parameters were then mean-centered and used as inputs for hierarchical principal components analysis (H-PCA, (61)). As a first step for H-PCA, PCA was carried out on the corrected amplitude, the corrected 'half-life' and the width. To account for the missing values introduced by employing cut-off values, the Non-linear Iterative Partial Least Squares (NIPALS)-PCA algorithm was used. The three resulting scores blocks were normalized by division by their highest values to give each 'scores block' equal importance and used as input variables for a second-level PCA.

RESULTS

Time Resolved Metabolic Footprinting (TReF) provides additional biological information compared to single time-point analysis

Initially, we monitored changes in Luria broth culture supernatant during the growth of the widely studied Gram-negative bacteria *Escherichia coli* (wild type MG1655) and *Pseudomonas aeruginosa* (wild types PA01, PA14 and the leucine auxotroph PA0381, which was derived from PA01 (17)). Additionally, growth of PA01 in a defined medium (SCFM) (46) was compared. The ^{1}H NMR spectra showed a complex mixture of small molecules, the majority of which could be readily assigned by comparison of their multiplicity and chemical shift to published or online values (Table 1). There were also a smaller number of resonances, which we have not yet assigned (0.91d, 1.07d, 1.19m, 1.27m, 1.36d, 2.69m, 3.81s, 5.85d, 5.88d, 6.03d, 6.08d, 6.15d, 6.30d, 6.86m).

Over the course of growth there were major changes in the metabolite composition of the growth media. This is illustrated in Fig. 1A, which shows the chemical shift region from 2 to 4 ppm of one LB grown culture of *P. aeruginosa* PA01 over time. At compound level, TReF revealed differences in the rates of uptake of individual compounds, as shown for three amino acids in a *P. aeruginosa* PA01 LB cultures. Alanine was taken up first from the medium, followed by threonine and then leucine (Fig. 1B). This clear time separation shows different modes of compound utilization during growth, and this differential compound utilization was observed for multiple compounds and in all investigated isolates. Further, the order in which compounds were utilized varied, but was reproducible at isolate level. These differences would

have been missed by single time-point profiling at 12 or 24 h and clearly indicate that comparative metabolomics would benefit from the application of TReF-based approaches, as differences can be highly growth-phase dependent.

Figure 2 provides a summary of the changes that were observed in the investigated cultures over time. Fig. 2A-E is a heatmap representation of averaged difference spectra depicting both uptake and secretion at compound level, clearly showing patterns of metabolite secretion and uptake that differed greatly between the different strains and media. Four different modes were identified. a) *Constant depletion*: the majority of metabolites in the medium decreased constantly over time (e.g. Fig. 1, Fig. 3B). b) *Transient excretion, followed by depletion*: some compounds (e.g. acetate, Fig. 2F) were excreted during one growth phase and taken up during another. c) *Transient depletion, followed by excretion*: all *Pseudomonas* strains first took up formate, only to excrete it at later time-points (Fig. 2H). d) *Constant excretion*: some compounds increased in a sigmoid fashion, e.g. an as-yet unassigned doublet resonance at δ 1.10 ppm (probable methyl group signal from an organic acid, Fig. 2G). As shown in Fig. 2, the growth medium itself has a large influence on the metabolite utilization and depletion patterns, with major differences between *P. aeruginosa* PA01 grown in LB and in SCFM. The uptake behavior at the compound level is summarized in Fig. 2 and Table 2. Based on these first observations, the differences in compound utilization and excretion were further investigated and are discussed below.

Non-linear regression modeling can be used to describe metabolite utilization over time

Most of the NMR-detectable resonances decreased over the course of growth (Fig 2I,J). In order to further describe the changes in exometabolome composition over time, the concentration changes of individual metabolites were modeled by regression. Linear regression against time was a poor descriptor of metabolite consumption. Most of the NMR resonance intensities did not describe a straight line when plotted against time and thus each modeled variable usually contained an unacceptable amount of fitting error (as an example, the dotted line in Fig. 3B shows the linear fit of the pyroglutamate resonance at 2.40 ppm in one *P. aeruginosa* PA01 culture). Only about one-third of the fitted resonances had an R^2 value greater than 0.6. For many compounds, the change in the resonance intensities roughly mirrored a growth curve and thus more closely resembled a straight line when plotted against OD (data not shown). The fits were indeed slightly improved when cell density (OD_{600}) rather than time was used as the X variable: about half the fitted resonances had R^2 values bigger than 0.6. However, the average correlation across all resonances was still poor for both time and OD (R=0.48 for time, 0.56 for OD). Instead, fits were significantly improved by using an appropriate non-linear model. A bacterial growth curve typically describes a sigmoid shape over time. Though the intensities of most NMR resonances did not exactly mirror this growth curve, they did decrease in a sigmoid fashion. Consequently, fitting sigmoid curves to the evolution of the resonances over time markedly decreased errors for 'real' peaks as opposed to noise (solid line in Fig. 3B). Even after imposing stringent cut-off values for fit (see methods), the dataset still contained about two-thirds of the resonances. Non-linear fitting is well suited to study media depletion, but was less useful for secreted metabolites.

For the data successfully fitted by non-linear modeling, the time course of each metabolite resonance was described by four parameters (Fig. 3A). Three parameters summarize the uptake characteristics for each metabolite: the relative decrease of the resonance with time (amplitude); the time of uptake (t50); and the duration of uptake (width). The fourth parameter, the offset, i.e. the intensity at the start of the experiment, does not represent meaningful information in this case, as we used difference spectra for the analysis. Hence, the offset was zero (for the original data) or close to zero (fitted data).

Uptake window plots visualize compound utilization

The parameters of the sigmoid equation can be used to obtain physiological information for individual compounds. Both the t_{50} and the width are in units of time with the t_{50} defining the time point at which the amplitude has reached its half-way point, i.e. when half of the compound has been utilized. The width is defined as the time that elapses for the exponent of e to go from 1 to -1 (see methods) and roughly translates to the duration in which the compound is taken up at the maximum rate, and thus defines a time span or “uptake window” for any fitted compound / resonance lying around the compound t_{50} value (Figure 3). These ‘uptake windows’ can be projected onto the OD_{600} growth curves of the individual strains to visualize differential compound uptake. Figures 4A-D show the projections of the uptake windows of seven compounds (alanine, leucine, threonine, asparagine, valine, succinate, and the disaccharide trehalose) onto the growth curves of the *E. coli* and the three *P. aeruginosa* strains for LB. Each circle represents the t_{50} value of one compound for one biological replicate with the bars on either side representing the width of the same compound.

These uptake window plots illustrate how TReF is able to elucidate similarities in and difference of compound utilization of strains, summarized with a single plot. Not only did the uptake windows differ dramatically for the individual metabolites, but there was very clear separation between them – i.e. the different amino acids fell into different 'utilization groups', which were separated along the growth curve. For example, *P. aeruginosa* PA01 (grown in LB) did not take up threonine until after the simultaneous depletion of alanine and asparagine. Leucine was then taken up after threonine had been removed. This order was also observed for the two other *P. aeruginosa* strains but was different in *E. coli*, with trehalose taken up before alanine, and leucine not taken up at all.

Additionally, the plots provide evidence for significant differences between the three *P. aeruginosa* strains. PA14 does not take up succinate in a sigmoidal fashion, however the compound was quickly removed from the medium in all strains. Interestingly, PA0381, originally derived from PA01, was shown to have lost its ability to utilize trehalose. This loss of function could be a side effect of the leucine auxotrophy causing a metabolic network rearrangement. However, a more parsimonious explanation is that the non-specific mutagenesis used to obtain the leucine auxotroph phenotype (53) also affected one of the genes necessary for trehalose breakdown (the transporter or the trehalase).

Transient changes in the exometabolome and metabolite excretion

Apart from metabolite uptake, a large proportion of the detected resonances transiently increased or decreased during growth in both LB and SCFM (Fig. 2). As a

positive confirmation, we detected acetate production by *E. coli*, a known example of overflow metabolism. Acetate is a fermentation product that accumulates at high growth rates, probably due to a rate bottleneck in aerobic metabolism (38); it was by far the clearest example of overflow metabolism in our current study. When grown in LB, all *Pseudomonas* strains transiently excreted the amino acids valine and tyrosine. In PA01 cultures, a singlet resonance at 2.24 ppm (putatively assigned as acetaldehyde) showed similar excretion dynamics to those of valine. Interestingly, this was not observed for the other *Pseudomonas* strains. In contrast, formate (Fig 2H) was taken up from the medium during the first couple of hours of growth, but was excreted in stationary phase. In addition to these transient changes, a number of resonances increased proportionally to cell number over the course of growth, including 6-hydroxynicotinate (all *Pseudomonas* strains), indole (*E. coli*), and uracil (all strains).

Compound utilization and excretion are dramatically influenced by the constituents of the growth media

It could be argued that the complexity of the responses we observed were partly down to our using a complex and undefined growth medium. To that end, we compared the exometabolome of *P. aeruginosa* PA01 grown in LB to that grown in SCFM, a defined medium designed and shown to mimic conditions and utilization dynamics in cystic fibrosis sputum (46). Even though the cell density (as OD_{600}) in different media did not differ greatly (data not shown), the choice of growth medium had a dramatic effect on the dynamics of the exometabolome, affecting both compound uptake and excretion (Figures 2 and 4E,F). Concerning compound utilization, a comparison of the uptake windows for selected amino acids in the two

media (Table 2 and Figure 4E,F) revealed several trends. Some amino acids, such as lysine, phenylalanine and leucine, were taken up later from LB than SCFM, which might hint at some sort of catabolite repression-like regulation in LB (see discussion). In contrast, the uptake dynamics of alanine, glutamate or aspartate and arginine were relatively unaffected as they were taken up at an early stage in both cultures. In terms of compound secretion, many more resonances increased when PA01 was grown in SCFM compared to LB. The transient increases in tyrosine and valine were also not observed in SCFM, but other resonances (1.07 d, 2.51 and 2.53 s) were observed to increase transiently. Finally, the pattern of formate change (transient decrease, followed by increase) was even more pronounced in SCFM.

Potential application of TReF as a functional genomics tool

Pattern recognition algorithms like PCA are widely used for multivariate data to visualize and summarize metabolic differences by dimension reduction. It was possible to separate *E. coli* and all *P. aeruginosa* strains using PCA on stationary phase samples and the approach very clearly showed the metabolites responsible for the strain differences (Fig. 5). However, the plots also show how single time-point profiling would miss the 'big picture', i.e. the metabolite concentration changes that occur at other time-points. If, for example, the cultures were sampled at 12 h, valine would appear to be excreted only by PA01 (Fig. 5E). In fact, PA14 and PA0381 also excrete valine at earlier time-points. Had the exometabolome been sampled at 24 h only, valine would appear to be utilized by all three *P. aeruginosa* strains to roughly the same extent. Additionally, the strains' leucine (Fig. 5F) utilization would look roughly equivalent after 12 h, whereas, in fact, leucine uptake was slower and had a slightly greater amplitude in PA01 cultures. Of the discriminatory metabolites at 12 h,

only trehalose (Fig. 5D) would show the same qualitative difference between the strain at all time-points. One advantage of the non-linear metabolite fitting is that the fit parameters summarize key biological endpoints (e.g. compound uptake rates) in a compact way. Thus, by using the fit parameters as input for the multivariate analyses, it is possible to compare data in a principled way from different strains, which might have slightly different growth rates, lag phase, etc. Naturally, each parameter could be analyzed separately, but it is also possible to combine these in a single hierarchical model (Fig. 5C).

As a test case for the resolution the TReF/H-PCA approach could offer, we analyzed culture supernatants of two species (nine strains in total) of the closely related *Burkholderia cepacia* complex. Single time-point profiling like that shown for stationary phase (t=24h) samples only provided some possible species separation, but with considerable overlap between the species groups (Fig. 6A, similar results for other time-points, data not shown). An added complication for this data set was that the strains showed large variations in growth rate, which were picked up by standard multivariate methods. However, the non-linear H-PCA approach showed a separation of *B. cepacia* and *B. cenocepacia* along PC1 (Fig. 6B). Thus, while 'standard' footprinting based on single time-points may be adequate for showing large metabolic differences, it failed to fully represent the subtle metabolic differences between the Bcc strains, which required the non-linear fit data. (We also tested H-PCA alone, i.e. a hierarchical model based on PCA for individual time-points without any curve fitting, but this offered no advantages in comparison to analyzing single time-points, and failed to separate the Bcc species; data not shown).

DISCUSSION

We have developed a time resolved metabolic footprinting approach for bacteria that should be widely applicable. Considering changes in the culture medium over the whole course of growth provides information that would be lost in a single time point analysis.

Bacteria show 'multiauxic' uptake behavior on complex media

TReF revealed differential compound uptake for all investigated strains, and for both a rich and a defined medium (LB and SCFM). The existence of a complex regulatory network leading to highly adaptable uptake dynamics is not surprising. In rich (or defined multi-compound) media, expression and translation of the transporter systems and catabolic pathways need to be controlled. The genomes of the *Pseudomonas* species group contain over 300 known or putative nutrient uptake systems (56). Expressing all inducible transporters and catabolic pathways at once will not be energetically favorable, and so a form of multiauxic growth and sequential compound uptake, like that observed here, is the likely outcome – although the extent of the differentiation between compound utilization classes during apparently exponential growth was surprising. A number of previous studies, albeit mostly not using rich media, have hinted at the complexity of the regulation at hand (e.g. 3, 19, 30).

Catabolite repression is a generic mechanism for regulation of substrate usage, and, for example, succinate represses arginine catabolism in *Pseudomonas aeruginosa* (42). ArgR controls the aerobic catabolism of arginine in *P. aeruginosa* (47), and also controls the levels of OprD, a porin for basic amino acids (44) and a serine

transporter (32). It is therefore logical that our data show that succinate depletion precedes the utilization of not only arginine, but also a number of other amino acids (Fig. 4). As a second example, lysine was depleted at an earlier growth phase in SCFM than in LB. Lysine can be imported by the specific permease LysP (54), but also by the putative basic amino acid ABC transporter PA5152-PA5155 (24). Transposon mutants within this operon were severely impaired in growth on ornithine as a single carbon source (24), so this transporter clearly contributes to *P. aeruginosa*'s ability to use ornithine. Hence it is highly probable that the high concentrations of ornithine in SCFM would induce expression of PA5152-PA5155, thereby potentially simultaneously increasing the potential rate of lysine uptake. These examples show how an untargetted approach can generate eminently testable hypotheses.

The influence of media composition on uptake and excretion

In addition to utilization, we studied compound excretion. Various compounds like acetate, valine and tyrosine were excreted transiently, whereas others like 6-hydroxy nicotinic acid or indole constantly increased over the course of growth for *P. aeruginosa* and *E. coli*, respectively. Formate had a particularly surprising utilization profile, with depletion followed by subsequent excretion; the precise reason is not clear at this moment. Compound excretion is a well-known phenomenon for biotechnologically interesting compounds in bacteria like *Corynebacterium glutamicum* (11, 40). A number of fundamental principles that lead to compound excretion have been formulated (11). The obvious explanation for a compound entering the culture medium is excretion of a product that bacteria "want" to excrete. This is the case for signaling molecules like quorum sensing (QS) signals. Our data

show excretion of indole in *E. coli*, which was suggested to have extracellular signaling properties (60). It should be noted that *P. aeruginosa* in particular is known for producing a suite of QS metabolites, which might be expected to be visible in the medium; the reason that we do not identify more QS-related changes is probably just that NMR has relatively high detection limits. However the TReF principle would be identical if using a more sensitive analytical platform, such as many techniques based on mass spectrometry. Additionally, compounds might also be excreted because of overflow metabolism, limited catabolism, and deregulated anabolism (11). This "relief-valve"-function has previously been suggested for the aromatic amino acid exporter (ArAE, formerly AaeAB) in *E. coli* (57). This transporter has recently been functionally annotated in *P. aeruginosa* (24), so tyrosine could be excreted by *P. aeruginosa* when grown in LB to relieve intracellular stress. Valine might be excreted due to similar reasons by a so-far unindentified transporter. Interestingly, tyrosine and valine were only excreted into LB, not SCFM. Finally, the increase of 6-hydroxynicotinic acid in *P. aeruginosa* cultures is probably due to limited catabolism of NAD or niacin, and has been used as a diagnostic marker of *P. aeruginosa* infection (20).

Species discrimination in the *Burkholderia cepacia* complex

An important and general question is to what degree *phenotypic* metabolomic data is informative about *genotype*, i.e. strain relatedness, as opposed to, say, ecotype, which could be a convergent result of adaptation. Previous studies have used both endo- and exometabolome profiling to address this in yeast and bacteria (33, 34, 48); it is clearly a complex question, as metabolomic data have shown both apparent

clustering by ecotype, with additional genetic within-cluster separation, and also high between-strain metabolic variability that mostly correlated with genotype divisions.

The *P. aeruginosa* and *E. coli* profiles were dramatically different, with the order of uptake of specific metabolites reversed (Fig. 4). However this is perhaps not surprising given these are very different organisms. We decided to carry out a more realistic test: whether differences could still be observed for a set of much more closely related bacteria. We chose two species of the Bcc (*Burkholderia cepacia* and *Burkholderia cenocepacia,* represented here by 4 and 5 independent isolates respectively) as a model comparison. The Bcc is a collection of genotypically distinct but phenotypically similar species within the genus *Burkholderia* (13, 37). Some Bcc members are opportunistic pathogens that can cause serious infections in patients with chronic granulomatous disease (CGD) or cystic fibrosis (35, 37), while some are found in the rhizosphere of important crops like maize and can protect these plants from fungal infection (5). Species-level identification of Bcc members is difficult and species are still frequently misidentified, especially using commercial identification systems (31). Single-gene phylogenies showed that *B. cepacia* and *B. cenocepacia* are especially similar genetically even within the Bcc (36, 55), meaning these two species formed a stringent test for our approach. The non-linear fitting TReF approach was nevertheless able to discriminate the isolates into species groups. It cannot be concluded at this point that this could therefore be used as a general tool for Bcc taxonomy (more isolates would need to be tested to derive robust conclusions about metabolic differences in these species), but serves as a proof-of-principle that our approach of modelling the full time course of metabolic changes

can provide additional and biologically meaningful data over single timepoint analyses.

Conclusion

We have shown potential microbiological applications of time-dependent exometabolome profiling. Modeling of the amino acid utilization of *E. coli* and *P. aeruginosa* demonstrated an unexpected complexity of regulation. In addition, the same approach was shown to have clear advantages over single-time point profiling. TReF allowed comparison of the physiology of bacteria in different nutritional environments, and our data clearly demonstrates that marked differences could be found. We believe time-dependent metabolic profiling could be a valuable addition to the fields of bacterial physiology, functional genomics, and as a tool for strain comparison, both as a complement to traditional taxonomies, and also for investigating properties such as strain-specific virulence. It is still likely that single-time-point metabolic footprinting will be preferred for many studies, simply because it requires analysis of fewer replicates. We see TReF having a complementary role, for in-depth phenotype analysis of a smaller number of strains – which might well, for instance, have been initially selected through single-time-point profiling.

Acknowledgements

VB was funded by a divisional studentship.

REFERENCES

1. **Allen, J., H. M. Davey, D. Broadhurst, J. K. Heald, J. J. Rowland, S. G. Oliver, and D. B. Kell**. 2003. High-throughput classification of yeast mutants for functional genomics using metabolic footprinting. Nat Biotechnol **21**:692-696.
2. **Allen, J., H. M. Davey, D. Broadhurst, J. J. Rowland, S. G. Oliver, and D. B. Kell**. 2004. Discrimination of modes of action of antifungal substances by use of metabolic footprinting. Appl Environ Microbiol **70**:6157-6165.
3. **Baev, M. V., D. Baev, A. J. Radek, and J. W. Campbell**. 2006. Growth of *Escherichia coli* MG1655 on LB medium: determining metabolic strategy with transcriptional microarrays. Appl Microbiol Biotechnol **71**:323-328.
4. **Beckonert, O., H. C. Keun, T. M. Ebbels, J. Bundy, E. Holmes, J. C. Lindon, and J. K. Nicholson**. 2007. Metabolic profiling, metabolomic and metabonomic procedures for NMR spectroscopy of urine, plasma, serum and tissue extracts. Nat Protoc **2**:2692-2703.
5. **Bevivino, A., V. Peggion, L. Chiarini, S. Tabacchioni, C. Cantale, and C. Dalmastri**. 2005. Effect of *Fusarium verticillioides* on maize-root-associated *Burkholderia cenocepacia* populations. Res Microbiol **156**:974-983.
6. **Bino, R. J., R. D. Hall, O. Fiehn, J. Kopka, K. Saito, J. Draper, B. J. Nikolau, P. Mendes, U. Roessner-Tunali, M. H. Beale, R. N. Trethewey, B. M. Lange, E. S. Wurtele, and L. W. Sumner**. 2004. Potential of metabolomics as a functional genomics tool. Trends Plant Sci **9**:418-425.

7. **Bolten, C. J., P. Kiefer, F. Letisse, J. C. Portais, and C. Wittmann**. 2007. Sampling for metabolome analysis of microorganisms. Anal Chem **79**:3843-3849.
8. **Buckstein, M. H., J. He, and H. Rubin**. 2008. Characterization of nucleotide pools as a function of physiological state in *Escherichia coli*. J Bacteriol **190**:718-726.
9. **Bundy, J. G., B. Papp, R. Harmston, R. A. Browne, E. M. Clayson, N. Burton, R. J. Reece, S. G. Oliver, and K. M. Brindle**. 2007. Evaluation of predicted network modules in yeast metabolism using NMR-based metabolite profiling. Genome Res **17**:510-519.
10. **Bundy, J. G., T. L. Willey, R. S. Castell, D. J. Ellar, and K. M. Brindle**. 2005. Discrimination of pathogenic clinical isolates and laboratory strains of *Bacillus cereus* by NMR-based metabolomic profiling. FEMS Microbiol Lett **242**:127-136.
11. **Burkovski, A., and R. Kramer**. 2002. Bacterial amino acid transport proteins: occurrence, functions, and significance for biotechnological applications. *Appl Microbiol Biotechnol* **58**:265-274.
12. **Canelas, A., C. Ras, P. ten, Angela, D. van, Jan, J. Heijnen, and G. van, Walter**. 2008. Leakage-free rapid quenching technique for yeast metabolomics. Metabolomics **4**:226-239.
13. **Chiarini, L., A. Bevivino, C. Dalmastri, S. Tabacchioni, and P. Visca**. 2006. Burkholderia cepacia complex species: health hazards and biotechnological potential. Trends Microbiol **14**:277-286.
14. **Cui, Q., I. A. Lewis, A. D. Hegeman, M. E. Anderson, J. Li, C. F. Schulte, W. M. Westler, H. R. Eghbalnia, M. R. Sussman, and J. L. Markley**. 2008.

Metabolite identification via the Madison Metabolomics Consortium Database. Nat Biotechnol **26**:162-164.

15. **de Koning, W., and K. van Dam**. 1992. A method for the determination of changes of glycolytic metabolites in yeast on a subsecond time scale using extraction at neutral pH. Anal Biochem **204**:118-123.
16. **Ebbels, T. M., H. C. Keun, O. P. Beckonert, M. E. Bollard, J. C. Lindon, E. Holmes, and J. K. Nicholson**. 2007. Prediction and classification of drug toxicity using probabilistic modeling of temporal metabolic data: the consortium on metabonomic toxicology screening approach. J Proteome Res **6**:4407-4422.
17. **Fyfe, J. A., and J. R. Govan**. 1980. Alginate synthesis in mucoid *Pseudomonas aeruginosa*: a chromosomal locus involved in control. J Gen Microbiol **119**:443-450.
18. **Goodacre, R., S. Vaidyanathan, W. B. Dunn, G. G. Harrigan, and D. B. Kell**. 2004. Metabolomics by numbers: acquiring and understanding global metabolite data. Trends Biotechnol **22**:245-252.
19. **Gschaedler, A., N. Thi Le, and J. Boudrant**. 1994. Glucose and acetate influences on the behavior of the recombinant strain *Escherichia coli* HB 101 (GAPDH). J Ind Microbiol **13**:225-232.
20. **Gupta, A., M. Dwivedi, G. A. Nagana Gowda, A. Ayyagari, A. A. Mahdi, M. Bhandari, and C. L. Khetrapal**. 2005. ^{1}H NMR spectroscopy in the diagnosis of *Pseudomonas aeruginosa*-induced urinary tract infection. NMR Biomed **18**:293-299.
21. **Hacker, J., and J. B. Kaper**. 2000. Pathogenicity islands and the evolution of microbes. Annu Rev Microbiol **54**:641-679.

22. **Hocquette, J. F**. 2005. Where are we in genomics? J Physiol Pharmacol **56 Suppl 3**:37-70.

23. **Holmes, E., F. W. Bonner, B. C. Sweatman, J. C. Lindon, C. R. Beddell, E. Rahr, and J. K. Nicholson**. 1992. Nuclear magnetic resonance spectroscopy and pattern recognition analysis of the biochemical processes associated with the progression of and recovery from nephrotoxic lesions in the rat induced by mercury(II) chloride and 2-bromoethanamine. Mol Pharmacol **42**:922-930.

24. **Johnson, D. A., S. G. Tetu, K. Phillippy, J. Chen, Q. Ren, and I. T. Paulsen**. 2008. High-throughput phenotypic characterization of *Pseudomonas aeruginosa* membrane transport genes. PLoS Genet **4**:e1000211.

25. **Kaderbhai, N. N., D. I. Broadhurst, D. I. Ellis, R. Goodacre, and D. B. Kell**. 2003. Functional genomics via metabolic footprinting: monitoring metabolite secretion by *Escherichia coli* tryptophan metabolism mutants using FT-IR and direct injection electrospray mass spectrometry. Comp. Funct. Genom. **4**:376-391.

26. **Kell, D. B**. 2006. Systems biology, metabolic modelling and metabolomics in drug discovery and development. Drug Discov Today **11**:1085-1092.

27. **Kell, D. B., M. Brown, H. M. Davey, W. B. Dunn, I. Spasic, and S. G. Oliver**. 2005. Metabolic footprinting and systems biology: the medium is the message. Nat Rev Microbiol **3**:557-565.

28. **Kell, D. B., and S. G. Oliver**. 2004. Here is the evidence, now what is the hypothesis? The complementary roles of inductive and hypothesis-driven science in the post-genomic era. Bioessays **26**:99-105.

29. **Konstantinidis, K. T., A. Ramette, and J. M. Tiedje**. 2006. The bacterial species definition in the genomic era. Philos Trans R Soc Lond B Biol Sci **361**:1929-1940.
30. **Lee, R., A. S. Ptolemy, L. Niewczas, and P. Britz-McKibbin**. 2007. Integrative metabolomics for characterizing unknown low-abundance metabolites by capillary electrophoresis-mass spectrometry with computer simulations. Anal Chem **79**:403-415.
31. **LiPuma, J. J**. 2007. Update on Burkholderia nomenclature and resistance. Clin. Microbiol. Newsletter **29**:65-69.
32. **Lu, C. D., Z. Yang, and W. Li**. 2004. Transcriptome analysis of the ArgR regulon in *Pseudomonas aeruginosa*. J Bacteriol **186**:3855-3861.
33. **Mackenzie, D. A., M. Defernez, W. B. Dunn, M. Brown, L. J. Fuller, S. R. de Herrera, A. Gunther, S. A. James, J. Eagles, M. Philo, R. Goodacre, and I. N. Roberts**. 2008. Relatedness of medically important strains of *Saccharomyces cerevisiae* as revealed by phylogenetics and metabolomics. Yeast **25**:501-512.
34. **Maharjan, R. P., and T. Ferenci**. 2005. Metabolomic diversity in the species *Escherichia coli* and its relationship to genetic population structure. Metabolomics **1**:235-242.
35. **Mahenthiralingam, E., A. Baldwin, and C. G. Dowson**. 2008. *Burkholderia cepacia* complex bacteria: opportunistic pathogens with important natural biology. J Appl Microbiol **104**:1539-1551.
36. **Mahenthiralingam, E., J. Bischof, S. K. Byrne, C. Radomski, J. E. Davies, Y. Av-Gay, and P. Vandamme**. 2000. DNA-Based diagnostic approaches for identification of *Burkholderia cepacia* complex, *Burkholderia vietnamiensis*,

Burkholderia multivorans, *Burkholderia stabilis*, and *Burkholderia cepacia* genomovars I and III. J Clin Microbiol **38**:3165-3173.

37. **Mahenthiralingam, E., T. A. Urban, and J. B. Goldberg**. 2005. The multifarious, multireplicon *Burkholderia cepacia* complex. Nat Rev Microbiol **3**:144-156.

38. **Majewski, R. A., and M. M. Domach**. 1990. Simple constrained-optimization view of acetate overflow in *E. coli*. Biotechnol Bioeng **35**:732-738.

39. **Majors, P. D., J. S. McLean, and J. C. Scholten**. 2008. NMR bioreactor development for live in-situ microbial functional analysis. J Magn Reson **192**:159-166.

40. **Mapelli, V., L. Olsson, and J. Nielsen**. 2008. Metabolic footprinting in microbiology: methods and applications in functional genomics and biotechnology. Trends Biotechnol **26**:490-497.

41. **Mas, S., S. G. Villas-Boas, M. E. Hansen, M. Akesson, and J. Nielsen**. 2007. A comparison of direct infusion MS and GC-MS for metabolic footprinting of yeast mutants. Biotechnol Bioeng **96**:1014-1022.

42. **Mercenier, A., J. P. Simon, D. Haas, and V. Stalon**. 1980. Catabolism of L-arginine by *Pseudomonas aeruginosa*. J Gen Microbiol **116**:381-389.

43. **Nicholson, J. K., J. Connelly, J. C. Lindon, and E. Holmes**. 2002. Metabonomics: a platform for studying drug toxicity and gene function. Nat Rev Drug Discov **1**:153-161.

44. **Ochs, M. M., C. D. Lu, R. E. Hancock, and A. T. Abdelal**. 1999. Amino acid-mediated induction of the basic amino acid-specific outer membrane porin OprD from *Pseudomonas aeruginosa*. J Bacteriol **181**:5426-5432.

45. **Oliver, S. G., M. K. Winson, D. B. Kell, and F. Baganz**. 1998. Systematic functional analysis of the yeast genome. Trends Biotechnol **16**:373-378.

46. **Palmer, K. L., L. M. Aye, and M. Whiteley**. 2007. Nutritional cues control *Pseudomonas aeruginosa* multicellular behavior in cystic fibrosis sputum. J Bacteriol **189**:8079-8087.

47. **Park, S. M., C. D. Lu, and A. T. Abdelal**. 1997. Cloning and characterization of argR, a gene that participates in regulation of arginine biosynthesis and catabolism in *Pseudomonas aeruginosa* PAO1. J Bacteriol **179**:5300-5308.

48. **Pope, G. A., D. A. MacKenzie, M. Defernez, M. A. Aroso, L. J. Fuller, F. A. Mellon, W. B. Dunn, M. Brown, R. Goodacre, D. B. Kell, M. E. Marvin, E. J. Louis, and I. N. Roberts**. 2007. Metabolic footprinting as a tool for discriminating between brewing yeasts. Yeast **24**:667-679.

49. **Raamsdonk, L. M., B. Teusink, D. Broadhurst, N. S. Zhang, A. Hayes, M. C. Walsh, J. A. Berden, K. M. Brindle, D. B. Kell, J. J. Rowland, H. V. Westerhoff, D. van, K, and S. G. Oliver**. 2001. A functional genomics strategy that uses metabolome data to reveal the phenotype of silent mutations. Nat Biotechnol **19**:45-50.

50. **Rahme, L. G., M. W. Tan, L. Le, S. M. Wong, R. G. Tompkins, S. B. Calderwood, and F. M. Ausubel**. 1997. Use of model plant hosts to identify *Pseudomonas aeruginosa* virulence factors. Proc Natl Acad Sci U S A **94**:13245-13250.

51. **Ryan, D., and K. Robards**. 2006. Metabolomics: The greatest omics of them all? Anal Chem **78**:7954-7958.

52. **Sariyar-Akbulut, B., A. Salman-Dilgimen, S. Ceylan, S. Perk, A. A. Denizci, and D. Kazan**. 2008. Preliminary phenotypic characterization of newly isolated

halophilic microorganisms by footprinting: a rapid metabolome analysis. Arch Microbiol **189**:19-26.

53. **Stanisich, V., and B. W. Holloway**. 1969. Conjugation in *Pseudomonas aeruginosa*. Genetics **61**:327-339.

54. **Steffes, C., J. Ellis, J. Wu, and B. P. Rosen**. 1992. The *lysP* gene encodes the lysine-specific permease. J Bacteriol **174**:3242-3249.

55. **Tabacchioni, S., L. Ferri, G. Manno, M. Mentasti, P. Cocchi, S. Campana, N. Ravenni, G. Taccetti, C. Dalmastri, L. Chiarini, A. Bevivino, and R. Fani**. 2008. Use of the *gyrB* gene to discriminate among species of the *Burkholderia cepacia* complex. FEMS Microbiol Lett **281**:175-182.

56. **Tamber, S., and R. E. Hancock**. 2003. On the mechanism of solute uptake in Pseudomonas. Front Biosci **8**:s472-83.

57. **Van Dyk, T. K., L. J. Templeton, K. A. Cantera, P. L. Sharpe, and F. S. Sariaslani**. 2004. Characterization of the *Escherichia coli* AaeAB efflux pump: a metabolic relief valve? J Bacteriol **186**:7196-7204.

58. **Viant, M. R., J. G. Bundy, C. A. Pincetich, J. S. de Ropp, and R. S. Tjeerdema**. 2005. NMR-derived developmental metabolic trajectories: an approach for visualizing the toxic actions of trichloroethylene during embryogenesis. Metabolomics **1**:149-158.

59. **Villas-Boas, S. G., and P. Bruheim**. 2007. Cold glycerol-saline: the promising quenching solution for accurate intracellular metabolite analysis of microbial cells. Anal Biochem **370**:87-97.

60. **Wang, D., X. Ding, and P. N. Rather**. 2001. Indole can act as an extracellular signal in *Escherichia coli*. J Bacteriol **183**:4210-4216.

61. **Westerhuis, J. A., T. Kourti, and J. F. MacGregor**. 1998. Analysis of multiblock and hierarchical PCA and PLS models. Journal of Chemometrics **12**:301-321.

62. **Winder, C. L., W. B. Dunn, S. Schuler, D. Broadhurst, R. Jarvis, G. M. Stephens, and R. Goodacre**. 2008. Global metabolic profiling of *Escherichia coli* cultures: an evaluation of methods for quenching and extraction of intracellular metabolites. Anal Chem **80**:2939-2948.

TABLES AND FIGURE LEGENDS

Table 1. List of assigned NMR-visible resonances in LB (note that the metabolites listed here may have other resonances: table includes only the most characteristic and well-resolved resonances). Resonances in bold font were used for non-linear fitting of compounds.

Compound	Assigned resonance frequency (ppm)					
Acetate[a]	**1.92**					
Acetaldehyde[a]	**2.24**					
Adenosine[a]	6.08	**8.26**	8.34			
Alanine[a]	**1.48**	3.79				
Arginine[a]	1.69	1.73	1.75	1.91	**3.25**	3.78
Asparagine[b]	1.72	**2.86**	2.96	4.00		
Aspartate[a]	2.68	**2.82**	3.91			
Formate[a]	**8.46**					
Glucose[a]	3.39	**5.24**				
Glutamate[a]	2.07	**2.35**	3.74			
Glycine[a]	**3.57**					
Glycine-betaine[a]	**3.27**	3.90				
Histidine (not fitted)[a]	3.11	3.14	3.31	7.07	7.88	
6-hydroxynicotinate[b]	**6.62**	8.07				
Indole[d]	**6.61**	7.18	7.27	7.42	7.56	7.72
Isoleucine[a]	**0.94**	1.01	1.25	1.26	3.68	3.74
Lactate[c]	**1.33**	4.12				
Leucine[a]	**0.96**	0.97	1.72	3.74		
Lysine[a]	1.46	1.48	1.73	1.89	1.91	**3.03**
Methionine[a]	2.12	2.14	**2.65**			
Methionine-S-oxide[b]	**2.74**	2.76	2.93			
Nicotinic acid[a]	**8.61**	8.94				
Pyrimidine nucleotide[a]	**5.91**					
Ornithine[c]	**3.81**					
Phenylalanine[a]	3.11	3.28	4.01	**7.33**	7.39	7.43
Pyroglutamate[b]	2.06	2.39	**2.42**	2.51	7.98	
Serine[a]	**3.79**	3.85	3.96			
Succinate[b]	**2.41**					
Threonine[a]	**1.33**	3.59	4.26			

Trehalose[a]	3.46	3.65	3.83	3.86	3.88	**5.20**
Tryptophan[b]	3.31	7.29	**7.55**	7.74		
Tyrosine[a]	3.07	3.22	3.31	3.94	**6.90**	7.20
Uracil[a]	**5.82**	7.55				
Valine[a]	0.99	**1.05**	2.28	3.62		
Unassigned metabolite (potential quinolone).	7.68	**8.10**				

a: observed in both LB and SCFM.

b: observed in LB only.

c: observed in SCFM only.

d: observed for *E. coli* only (not tested in SCFM).

Table 2. Comparison of fitted metabolite t_{50} values (h) for *P. aeruginosa* PA01 grown in LB and SCFM.

	LB	SCFM	Difference[a]
Tyrosine	14.8	6.5	-8.3
Valine	15.8	8.5	-7.3
Phenylalanine	8.8	5.0	-3.8
Lysine	11.3	8.0	-3.3
Leucine	9.6	7.0	-2.5
Isoleucine	8.1	7.0	-1.2
Aspartate	3.1	2.2	-0.9
Arginine	4.0	3.5	-0.5
Glycine	5.3	5.0	-0.3
Glutamate	2.9	2.8	-0.2
Alanine	3.5	3.4	-0.1
Serine	2.7	4.3	1.6
Threonine	5.8	7.7	2.0
Asparagine	2.3	not observed	-
Methionine	not utilized	11.8	-
Ornithine	not observed	4.0	-
Tryptophan	4.7	not observed	-

a: 'Difference' refers to difference between t_{50} in SCFM compared to LB medium, i.e. the lower the value, the earlier metabolite was taken up in SCFM compared to LB.

Figure 1. A: section of 600 MHz ^{1}H NMR spectra (4—2 ppm) for a single *P. aeruginosa* PA01 culture over a growth curve. Time-specific metabolic changes are clearly seen. B: single compound utilization data for three selected metabolites for *P. aeruginosa* PA01. Error bars = SEM (n = 4).

Figure 2: Metabolite changes in different media and different strains across the course of growth. Heatmaps (panels A – E): each row represents a metabolite, or a peak from an as-yet unassigned metabolite. Blue represents decrease in concentration, and red represents increase in concentration. Note that panels B – E can be directly compared visually, but the metabolites in panel A do not line up directly with B – E. Row for metabolite '6HN / indole' represents 6-hydroxynicotinate for *P. aeruginosa* strains, and indole for *E. coli*.

A: *P. aeruginosa* PA01, synthetic cystic fibrosis medium.

B: *P. aeruginosa* PA01, LB.

C: *P. aeruginosa* PA14, LB.

D: *P. aeruginosa* PA0381, LB.

E: *E. coli*, LB.

Selected metabolites with different modes of utilization/production are then shown in detail in the bottom half of the figure (error bars represent ± SEM):

F: acetate, *E. coli*. Transient increase in metabolite concentration.

G: unassigned metabolite, *E. coli*, peak at δ 1.10 ppm. Steady increase in metabolite concentration.

H: formate, *P. aeruginosa* PA01, LB. Transient decrease in metabolite concentration followed by subsequent production.

An overall comparison of the different modes is then shown as pie charts (percentage of assigned metabolites that change in some way during growth).

I: *P. aeruginosa* PA01, SCFM.

J: *P. aeruginosa* PA01, LB.

Figure 3. A: Schematic showing the parameters for non-linear curve fitting. B (inset): curve fit for a representative compound (pyroglutamate) for *P. aeruginosa* PA01. Solid line indicates sigmoid fit; dotted line indicates much poorer linear fit.

Figure 4. Uptake window plots for seven example compounds for all four bacterial strains. Compound t_{50} is back-projected upon the actual culture growth curve, i.e. all biological replicates are shown. The 'error bars' represent calculated width (see Fig. 2 for illustration of t_{50} and width). Note that both abscissa (time) and ordinate (OD_{600}) have been scaled such that growth curve maxima are set at 100%, to facilitate comparison across different strains. A: *E. coli*. B: *P. aeruginosa* PA01. C: *P. aeruginosa* PA14. D: *P. aeruginosa* PA0381. The remaining two panels compare uptake windows for *P. aeruginosa* PA01 for two different media, LB and synthetic cystic fibrosis medium (SCFM). Note that glucose is plotted (not trehalose as for panel A), as glucose is higher concentration in SCFM. E: F:

Figure 5. A: Principal components analysis for 12 h data, scores plot of axes 1 and 2. Filled circles: *E. coli*. Empty circles: *P. aeruginosa* PA01. Empty triangles: *P. aeruginosa* PA14. Empty squares: *P. aeruginosa* PA0381. PCs 1 and 2 explained 87% and 8% of the variance in the data, respectively.

B: loadings plot for analysis shown in A. Variables corresponding to assigned metabolite bins for leucine, valine, and trehalose are labelled directly on the plot.

C: Hierarchical principal components analysis of fitted time-course data. Figure symbols are the same as for A. PCs 1 and 2 explained 50% and 33% of the variance in the data, respectively.

D: Trehalose utilization during growth for four strains. Solid black line: *E. coli*. Solid grey line: *P. aeruginosa* PA01. Dashed line (long dashes): *P. aeruginosa* PA14. Dashed line (short dashes): *P. aeruginosa* PA0381.

E: Valine utilization during growth for four strains. Line styles as for D.

F: Leucine utilization during growth for four strains. Line styles as for D.

Figure 6. Comparison of single-timepoint and nonlinear fitted metabolite data for four *Burkholderia cepacia* (unfilled symbols) and five *Burkholderia cenocepacia* (filled symbols) isolates: principal components scores plots, axis 1 v axis 2. Different symbol shapes represent different individual isolates.

A: Single-timepoint analysis does not discriminate all isolates into species. PCs 1 and 2 explained 55% and 39% of the variance in the data, respectively.

B: Fitted metabolite data (TReF) shows that species are discriminated along PC 1 across different isolates. PCs 1 and 2 explained 35% and 25% of the variance in the data, respectively.

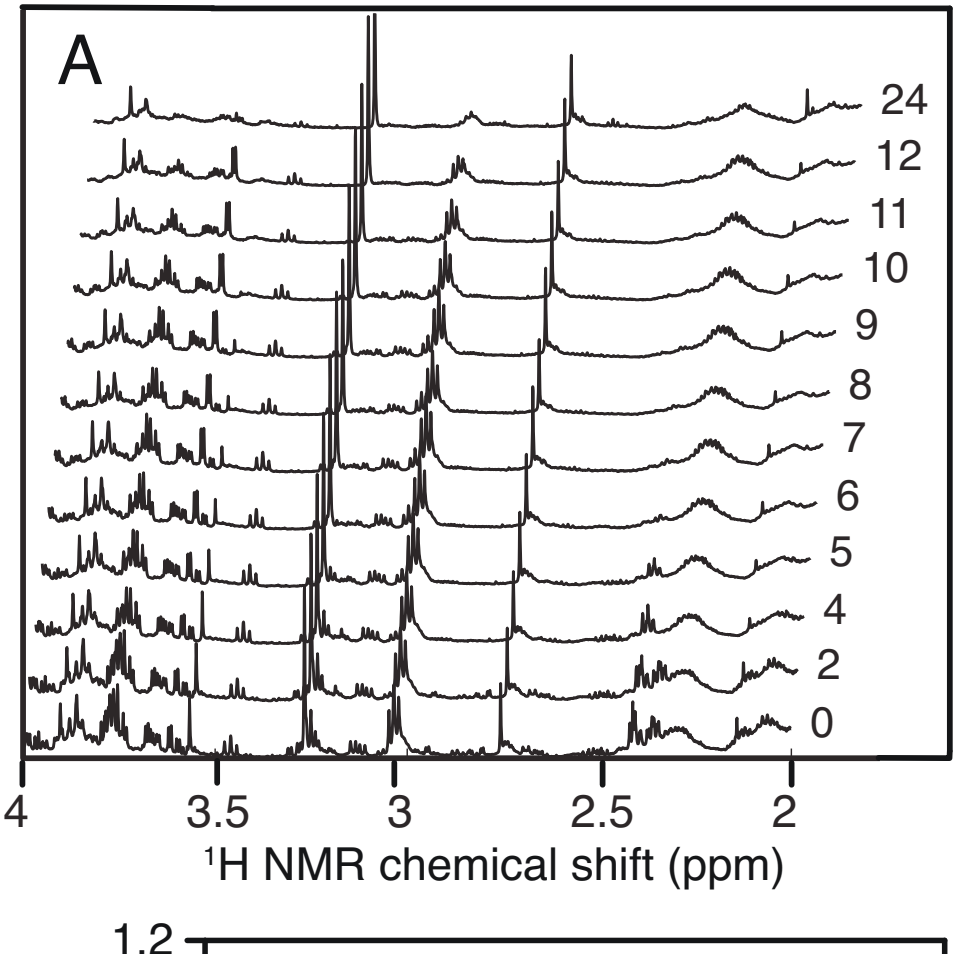
A
24
12
11
10
9
8
7
6
5
4
2
0
4
3.5
3
2.5
2
¹H NMR chemical shift (ppm)

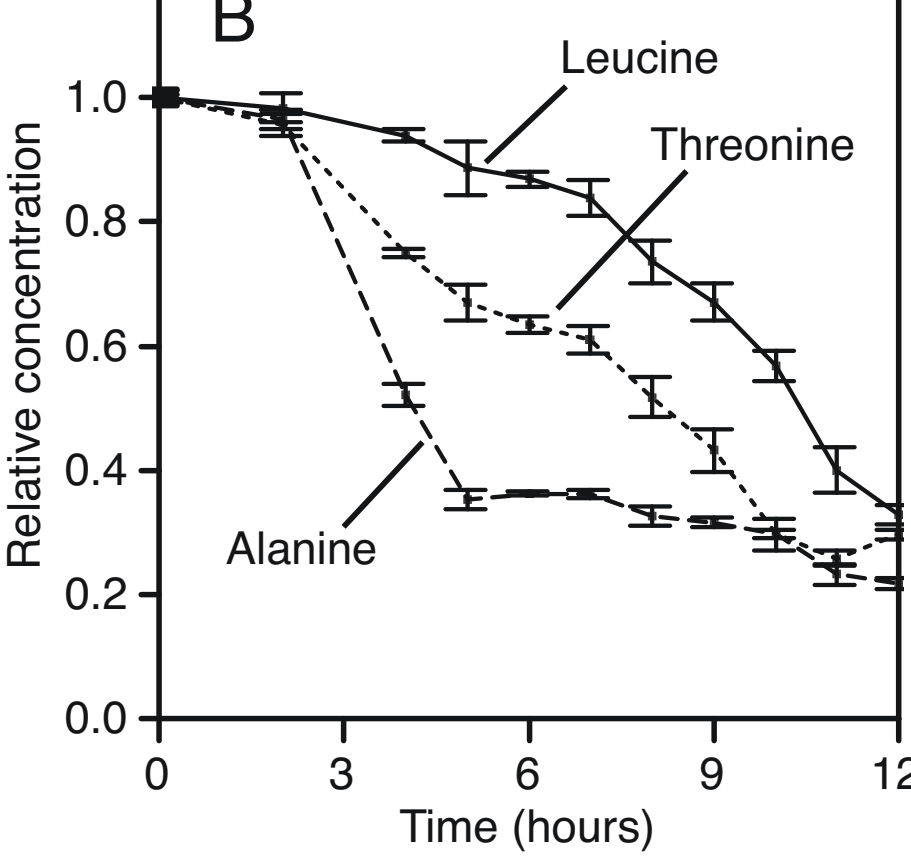
B
Leucine
Threonine
Alanine
Relative concentration
1.2
1.0
0.8
0.6
0.4
0.2
0.0
0
3
6
9
12
Time (hours)

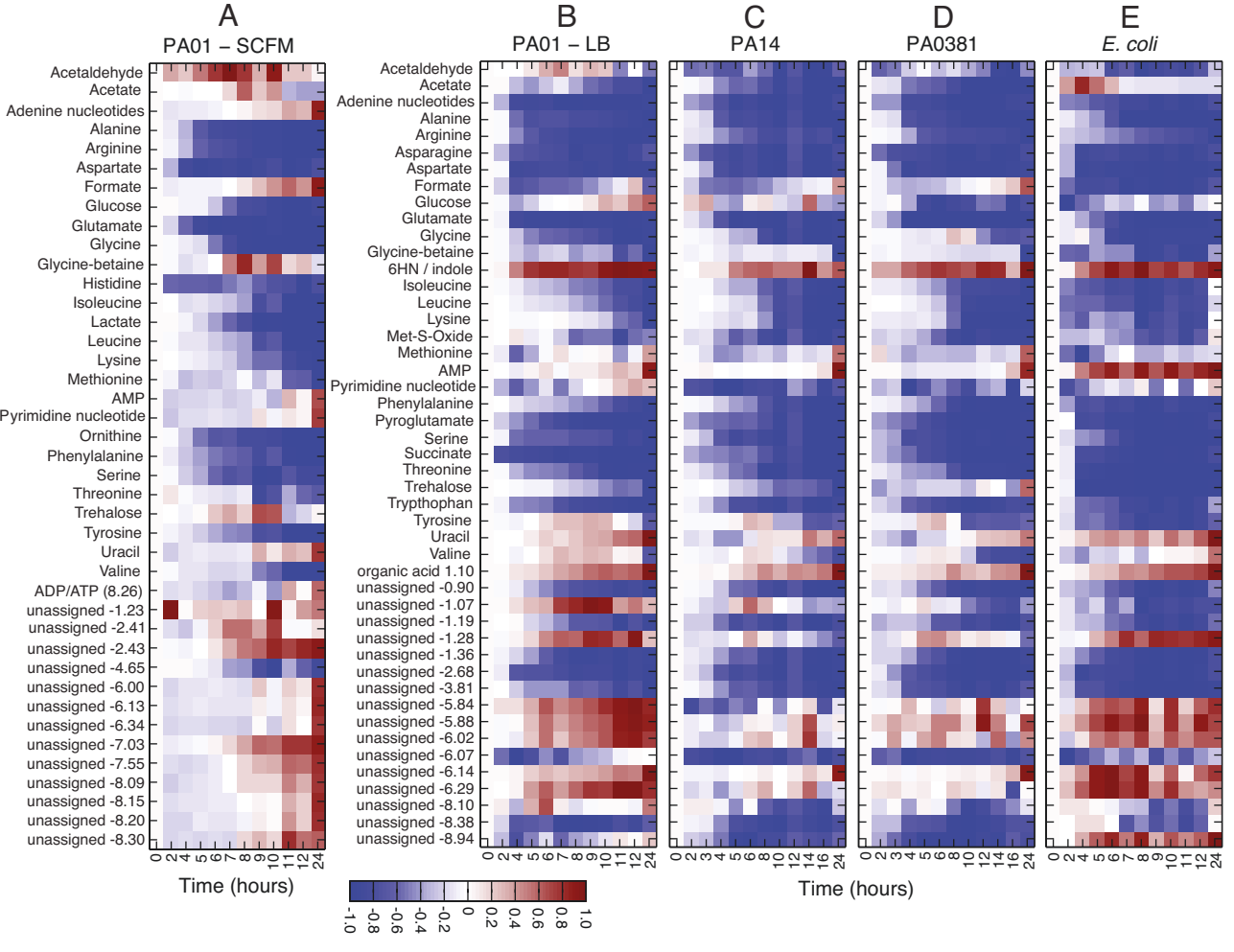
A
PA01 – SCFM
B
PA01 – LB
C
PA14
D
PA0381
E
E. coli
Acetaldehyde
Acetate
Adenine nucleotides
Alanine
Arginine
Asparagine
Aspartate
Formate
Glucose
Glutamate
Glycine
Glycine-betaine
6HN / indole
Histidine
Isoleucine
Lactate
Leucine
Lysine
Met-S-Oxide
Methionine
AMP
Pyrimidine nucleotide
Ornithine
Phenylalanine
Pyroglutamate
Serine
Succinate
Threonine
Trehalose
Trypthophan
Tyrosine
Uracil
Valine
organic acid 1.10
ADP/ATP (8.26)
unassigned -0.90
unassigned -1.07
unassigned -1.19
unassigned -1.23
unassigned -1.28
unassigned -1.36
unassigned -2.41
unassigned -2.43
unassigned -2.68
unassigned -3.81
unassigned -4.65
unassigned -5.84
unassigned -5.88
unassigned -6.00
unassigned -6.02
unassigned -6.07
unassigned -6.13
unassigned -6.14
unassigned -6.29
unassigned -6.34
unassigned -7.03
unassigned -7.55
unassigned -8.09
unassigned -8.10
unassigned -8.15
unassigned -8.20
unassigned -8.30
unassigned -8.38
unassigned -8.94
Time (hours)
Time (hours)
-1.0
-0.8
-0.6
-0.4
-0.2
0
0.2
0.4
0.6
0.8
1.0

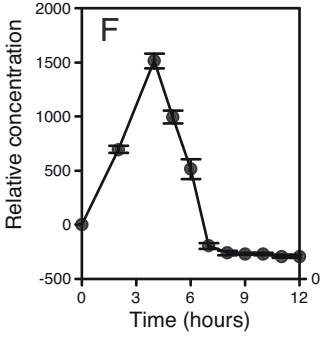
F
Relative concentration
Time (hours)

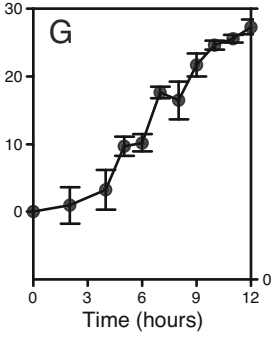
G
Time (hours)

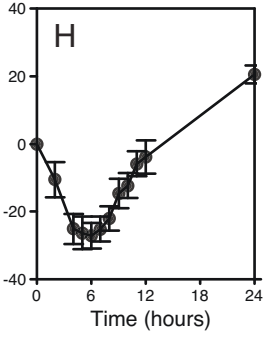
H
Time (hours)

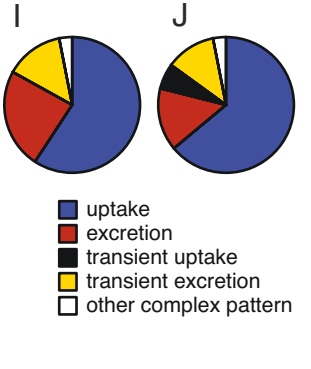
I
J
uptake
excretion
transient uptake
transient excretion
other complex pattern

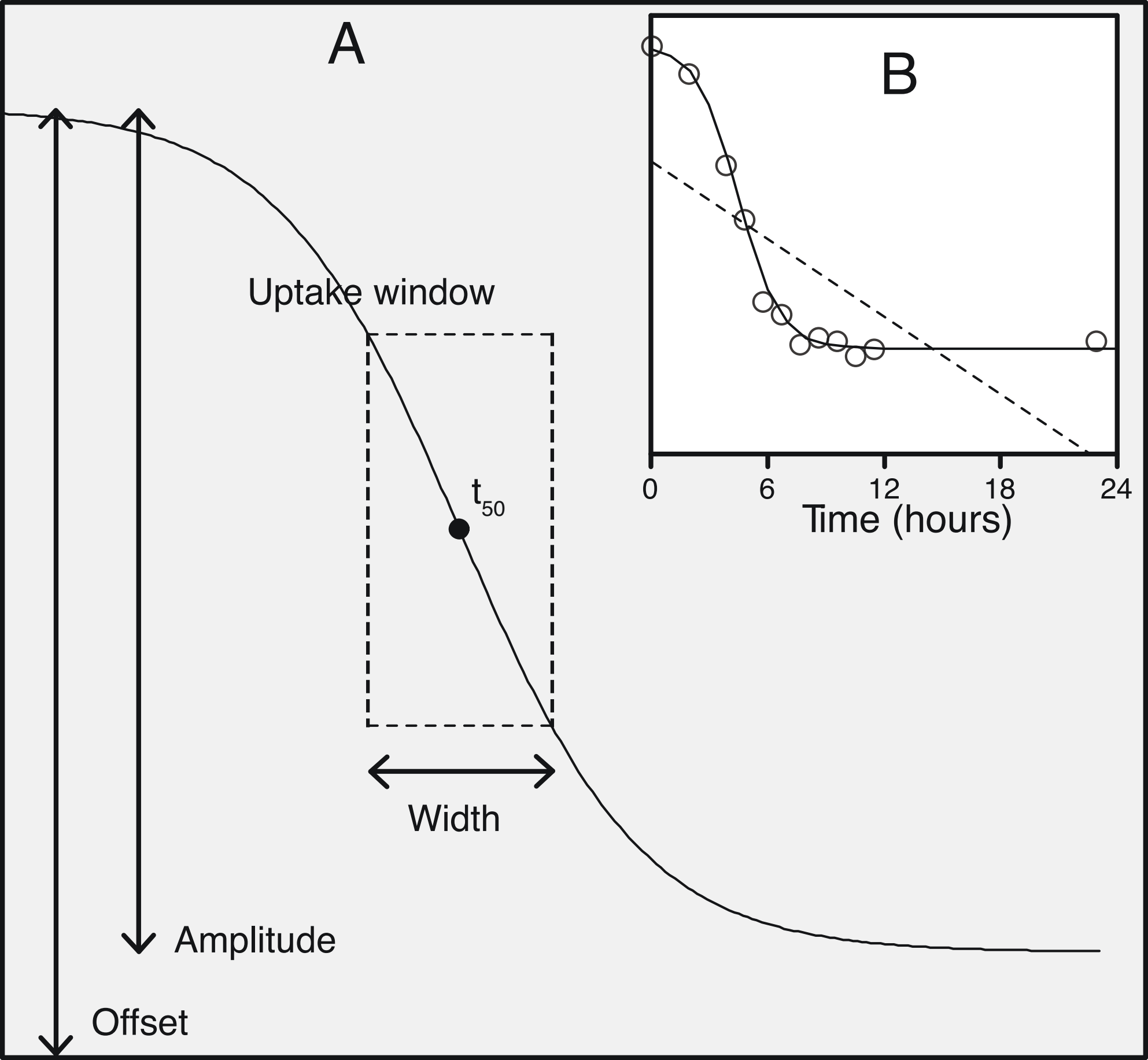
A
B
Uptake window
t_{50}
Width
Amplitude
Offset
0
6
12
18
24
Time (hours)

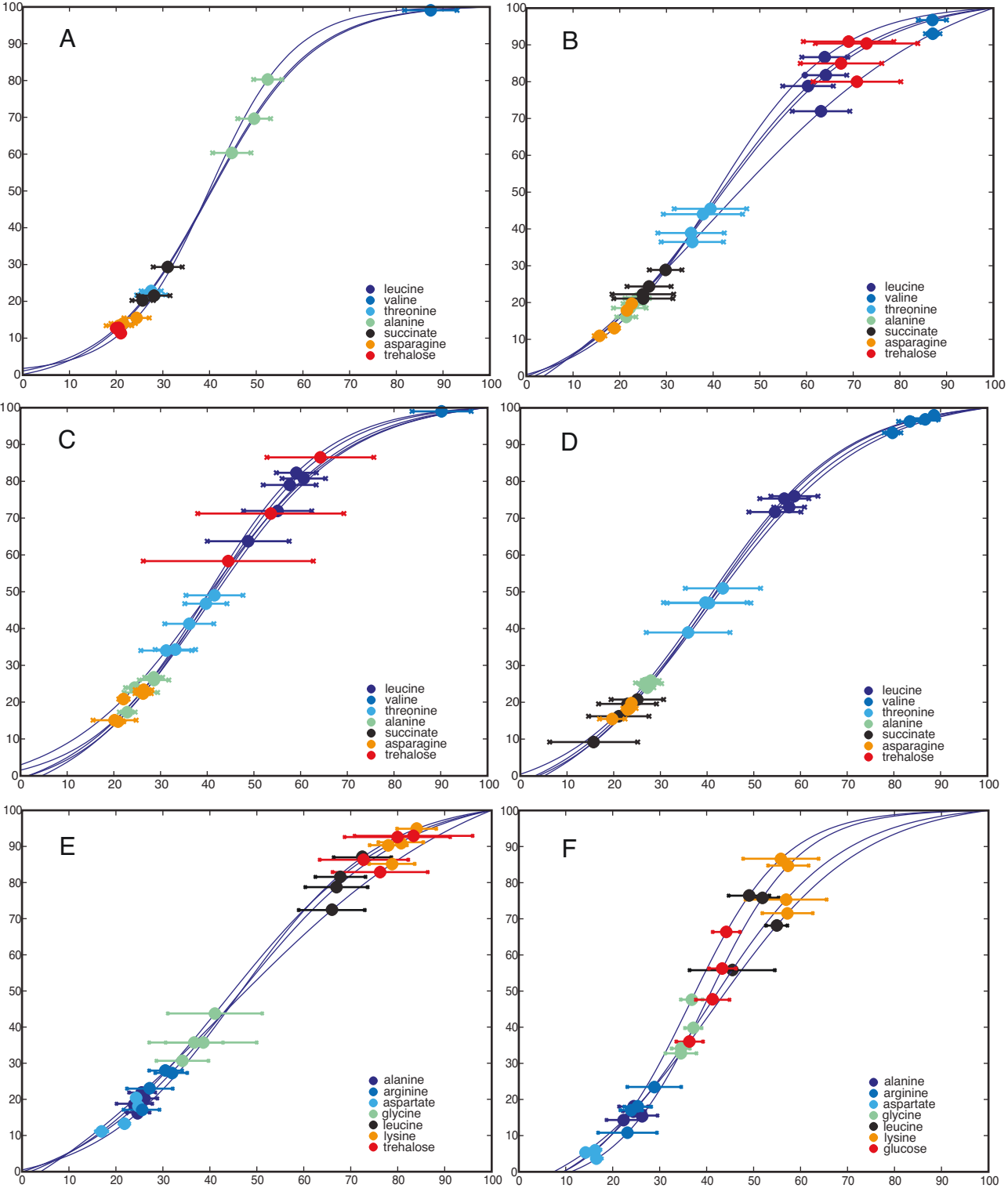
A
leucine
valine
threonine
alanine
succinate
asparagine
trehalose
B
leucine
valine
threonine
alanine
succinate
asparagine
trehalose
C
leucine
valine
threonine
alanine
succinate
asparagine
trehalose
D
leucine
valine
threonine
alanine
succinate
asparagine
trehalose
E
alanine
arginine
aspartate
glycine
leucine
lysine
trehalose
F
alanine
arginine
aspartate
glycine
leucine
lysine
glucose

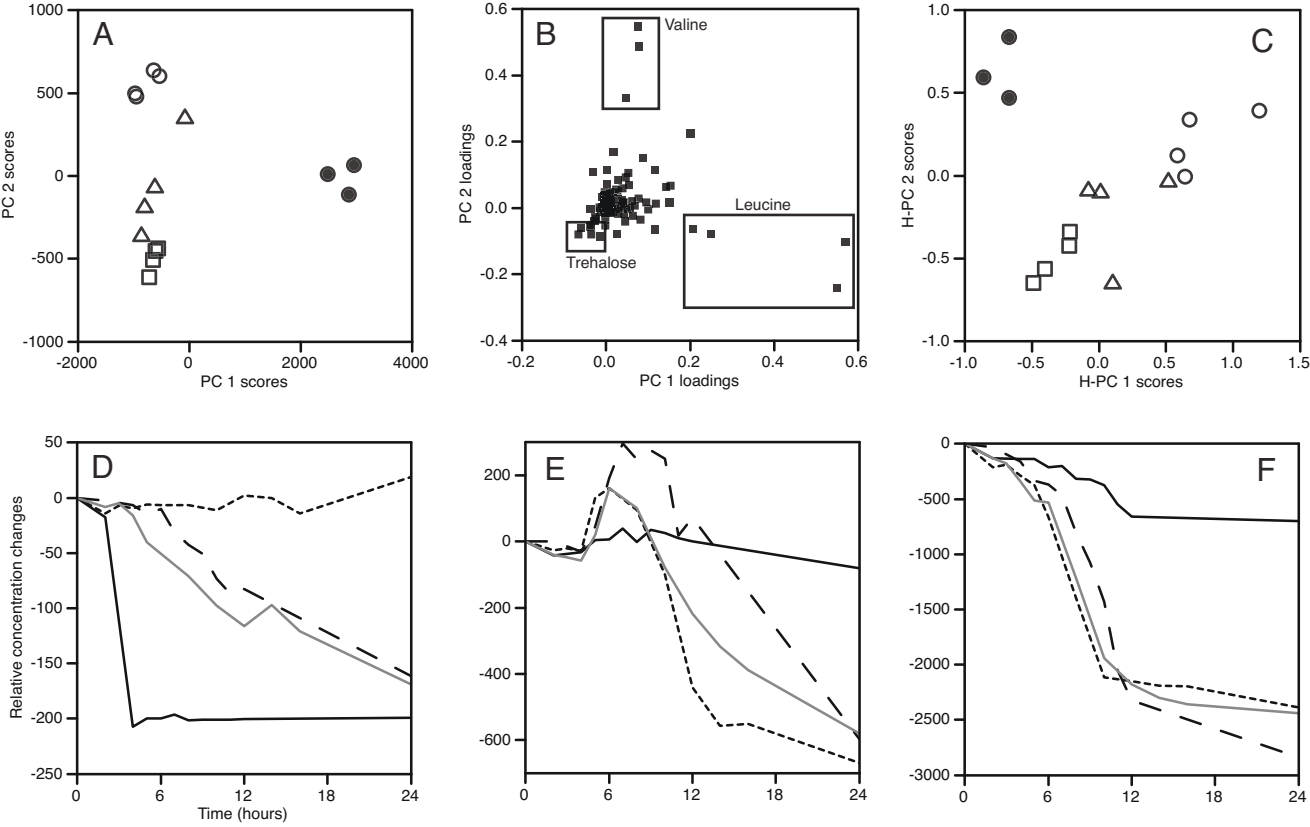
A
PC 2 scores
PC 1 scores
B
Valine
Leucine
Trehalose
PC 2 loadings
PC 1 loadings
C
H-PC 2 scores
H-PC 1 scores
D
Relative concentration changes
Time (hours)
E
F

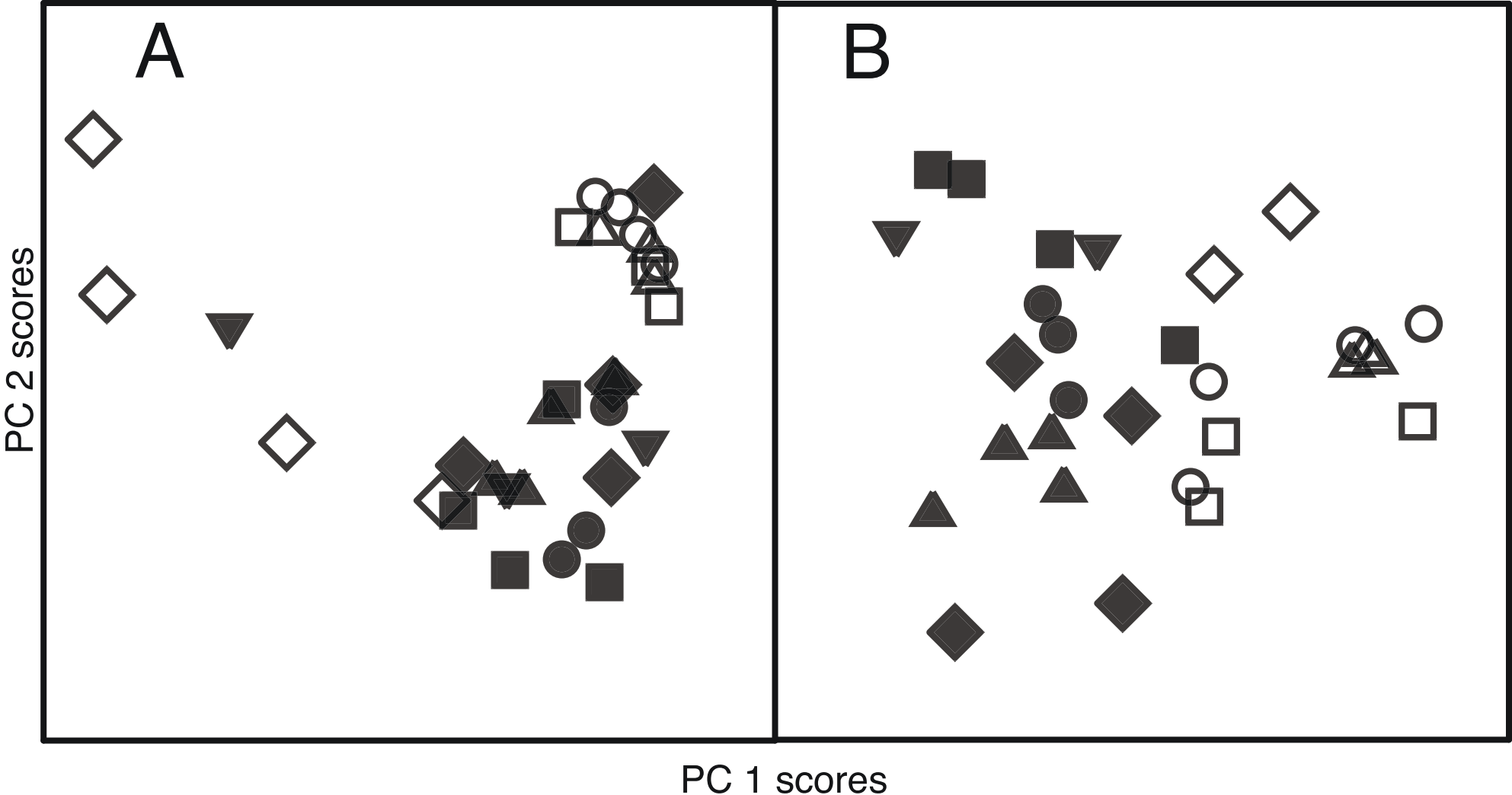
A
B
PC 2 scores
PC 1 scores